

Ultra wide sensing range plasmonic refractive index sensor based on nano-array with rhombus particles

Jiankai Zhu(朱剑凯), Xiangxian Wang(王向贤), Xiaoxiong Wu(吴枭雄), Yingwen Su(苏盈文), Yueqi Xu(徐月奇), Yunping Qi(祁云平), Liping Zhang(张丽萍), Hua Yang(杨华)

Citation: Chin. Phys. B . 2020, 29(11): 114204 . **doi:** 10.1088/1674-1056/abb229
Journal homepage: http://cpb.iphy.ac.cn; http://iopscience.iop.org/cpb

What follows is a list of articles you may be interested in

A theoretical study of a plasmonic sensor comprising a gold nano-disk array on gold film with a SiO_2 spacer

Xiangxian Wang(王向贤), Jiankai Zhu(朱剑凯), Huan Tong(童欢), Xudong Yang(杨旭东), Xiaoxiong Wu(吴枭雄), Zhiyuan Pang(庞志远), Hua Yang(杨华), Yunping Qi(祁云平)

Chin. Phys. B . 2019, 28(4): 044201 . **doi:** 10.1088/1674-1056/28/4/044201

Analysis of optical properties of bio-smoke materials in the 0.25-14 μm band

Xinying Zhao(赵欣颖), Yihua Hu(胡以华), Youlin Gu(顾有林), Xi Chen(陈曦), Xinyu Wang(王新宇), Peng Wang(王鹏), Xiao Dong(董骁)

Chin. Phys. B . 2019, 28(3): 034201 . **doi:** 10.1088/1674-1056/28/3/034201

Cascaded tilted fiber Bragg grating for enhanced refractive index sensing

Biqiang Jiang(姜碧强), Zhixuan Bi(毕芷瑄), Shouheng Wang(王守恒), Teli Xi(席特立), Kaiming Zhou, Lin Zhang, Jianlin Zhao(赵建林)

Chin. Phys. B . 2018, 27(11): 114220 . **doi:** 10.1088/1674-1056/27/11/114220

Coherently induced grating in refractive index enhanced medium

Zhuan-Zhuan Liu(刘撰撰), Yu-Yuan Chen(陈煜远), Jia-Yu Yuan(原佳宇), Ren-Gang Wan(万仁刚)

Chin. Phys. B . 2017, 26(12): 124209 . **doi:** 10.1088/1674-1056/26/12/124209

Apodized grating coupler using fully-etched nanostructures

Hua Wu(武华), Chong Li(李冲), Zhi-Yong Li(李智勇), Xia Guo(郭霞)

Chin. Phys. B . 2016, 25(8): 084212 . **doi:** 10.1088/1674-1056/25/8/084212

Ultra wide sensing range plasmonic refractive index sensor based on nano-array with rhombus particles*

Jiankai Zhu(朱剑凯)[1], Xiangxian Wang(王向贤)[1,†], Xiaoxiong Wu(吴枭雄)[1], Yingwen Su(苏盈文)[1], Yueqi Xu(徐月奇)[1], Yunping Qi(祁云平)[2], Liping Zhang(张丽萍)[1], and Hua Yang(杨华)[1]

[1] *School of Science, Lanzhou University of Technology, Lanzhou* 730050, *China*
[2] *College of Physics and Electronic Engineering, Northwest Normal University, Lanzhou* 730070, *China*

(Received 11 June 2020; revised manuscript received 29 June 2020; accepted manuscript online 25 August 2020)

We propose a two-dimensional metal grating with rhombus particles on a gold film structure for refractive index sensing due to its perfect absorption at near-infrared wavelength. Via two-dimensional metal grating coupling, the incident light energy is effectively transformed into the surface plasmons which propagate along the upper surface of the gold film and interact with the surrounding environment in a wide range. The plasmonic resonance mechanism of the structure is discussed in detail by theoretical analysis and finite-difference time-domain method. After optimizing the geometrical parameters, the designed structure shows the sensing performance with a refractive index sensitivity of 1006 nm/RIU. More importantly, this plasmonic refractive index sensor achieves an ultra wide refractive index sensing range from 1.0 to 2.4 with a stable sensing performance. The promising simulation results of the structure show that the sensor has a broad application prospect in the field of biology and chemistry.

Keywords: plasmonic sensor, refractive index, sensitivity, figure of merit (FOM)

PACS: 42.25.Bs, 42.25.–p, 42.79.–e **DOI:** 10.1088/1674-1056/abb229

1. Introduction

In the last decade, the rapid development of various micro-nano processing technologies, including physical and chemical methods, has made increasingly complex micro-nano structures a reality. Concurrently, it lays a solid foundation for the wide application of micro-nano structures such as in solar absorption,[1–4] photonic crystal,[5–7] optical waveguides,[8,9] electrode material,[10,11] photocatalysis,[12–16] and other applications.[17–22] Generally, the designed micro-nano structures have a very attractive application prospect in the optical field due to their ability to control the diffraction and propagation of light to a certain extent. When the metal containing a large number of free electrons is involved in the micro-nano structure, the surface plasmon phenomenon can be produced under the excitation of external electromagnetic wave. Surface plasmon on metal micro-nano structure is an important research field of micro-nano optics. Its applications include but are not limited to photolithography,[23,24] absorber,[25–27] filter,[28–30] surface enhanced Raman,[31–34] and photonic crystal fibers.[35–37] Optical sensor based on surface plasmon resonance (SPR) is a strongly active field in recent years[38–42] due to the advantages of high-sensitivity, rapid, specific, and real-time compare with traditional biological/chemical sensors. Especially the SPR sensor has the advantages of miniaturization and integration,[43] which make it pretty consistent with the concept of portable devices in the future.

SPR is usually subdivided into propagation surface plasmon (PSP) resonance and localized surface plasmon (LSP) resonance, and they both can be used for refractive index (RI) sensing. The RI sensor based on PSP resonance usually has higher sensitivity and figure of merit (FOM), but its excitation often needs an additional prism structure, which makes integration difficult. LSP resonance can be excited directly by electromagnetic wave, but the wider full width at half maximum (FWHM) results in lower FOM and spectral resolution of the RI sensor. In order to solve the above contradiction, the integrated nano-grating can be used instead of the prism to excite the PSP of the metal film. In fact, numerous research works on the SPR-based RI sensor in recent years are related to the nano-grating.[38–45] In 2019, Sun *et al.* proposed a plasmonic perfect absorber based on two-dimensional dielectric–metal grating and applied as a RI sensor,[44] which is able to achieve the RI sensitivity of 526 nm/RIU and a FOM of 73.1 RIU^{-1}. At the same year, a plasmonic RI sensor only based on gold/silicon Schottky junction (also a one-dimensional grating) was designed with a RI sensitivity of over 1000 nm/RIU after parameter optimization.[45] Nevertheless, the sensing range in many works was mostly considered near the liquid (the RI is around 1.33), or they could not maintain a good sensing performance in a wide range of RI.

In our previous work, we proposed a composite structure of a gold nanocube array coupled to a gold mirror for RI

*Project supported by the National Natural Science Foundation of China (Grant Nos. 61865008 and 61505074) and the HongLiu First-Class Disciplines Development Program of Lanzhou University of Technology.

†Corresponding author. E-mail: wangxx869@lut.edu.cn

© 2020 Chinese Physical Society and IOP Publishing Ltd

sensing.[46] However, the sensing limit of the composite structure requires the RI of the analyte to be less than 1.8 due to the anticrossing behavior between different resonance modes. In this work, we further optimize the unit of two-dimensional (2D) grating and directly located the 2D grating on the gold film without any spacers. Hence, a plasmonic RI sensor with high sensitivity, high FOM, wider sensing range (the RI of analyte can even exceed 2.4), and simpler fabrication process is realized. The simulation results show that the structure we designed can effectively couple the energy of incident light to the interface between analyte and metal (formed PSP). The resonance peak with narrow FWHM observed in the absorption spectrum makes it very suitable for RI sensing. The geometric parameters of the structure most helpful for RI sensing are also discussed. Finally, we describe the sensing performance of the structure via important physical parameters including sensitivity, FOM, and sensing range.

2. Structure and materials

The considered structure based on 2D metal grating is illustrated in Fig. 1, which consists of periodic arrays of gold particles and a gold film on the glass substrate. The periodic array is situated directly on the gold film. Here, we assume that the periods in X and Y directions are equal, which is the distance between the nearest two particle centers. The units that make up the 2D grating are the rhombus particles. As shown in the enlarged view in Fig. 1, the main geometric parameters of the rhombus particles are the internal angle θ and side length w of rhombus and the height h_1 of the particle. For simplicity, the θ of the rhombus and the thickness h_2 of the gold film are set at 60° and 100 nm, respectively. In the practical structure fabrication, a layer of gold film is first deposited on a glass substrate by magnetron sputtering. Then, a photoresist is coated on the gold film and rhombus holes are fabricated by electron beam lithography. After that, gold is deposited again by magnetron sputtering. Finally, the photoresist is removed by the lift-off process, leaving 2D gold grating on a gold film. It should be pointed out that due to the existence of gold film reflector, the transmittance of the structure is almost eliminated in the whole near-infrared band. The dielectric constant of gold is selected from the experimental data supported by the Drude model.[47] The surrounding RI is assumed to be 1 unless indicated. The surface plasmons of the structure are excited vertically by linearly polarized light with the direction of polarization along the periodic direction, as shown by the black and blue arrows in the figure.

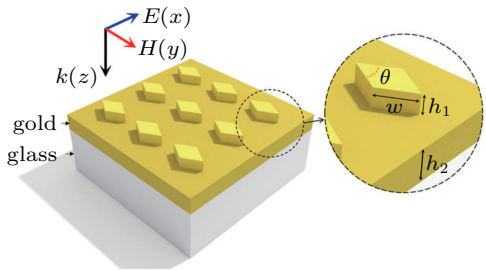


Fig. 1. Schematic view of the proposed plasmonic structure. From top to bottom, the components consist of 2D gold periodic arrays, gold film, and glass substrate. The black and blue arrows represent the propagation direction and polarization direction of the incident light, respectively. Inside the dotted circle shows the enlarged view of the rhombus particles.

3. Plasmonic response of the structure

Before applying the structure to the SPR sensor, it is necessary to discuss the plasmonic responses of the designed structure. Figure 2 illustrates the absorption spectrum of the structure in the near-infrared waveband when $w = 380$ nm, $h_1 = 80$ nm, and the 2D grating period is 1000 nm. Two main SPR modes can be observed clearly and mode 2 shows a perfect absorption at the wavelength of ~ 1007 nm. It should be noted that mode 2 is very suitable for RI sensing due to its narrow FHWM and high peak strength (the peak strength is defined as the difference between the highest and lowest absorptivity of the resonance peak as shown by the red dotted line in Fig. 2), which means good performance in FOM and therefor better spectral resolution. Considering the periodic array in the structure, modes 1 and 2 can be attributed to the compensation of optical momentum via 2D metal grating with different diffraction orders.

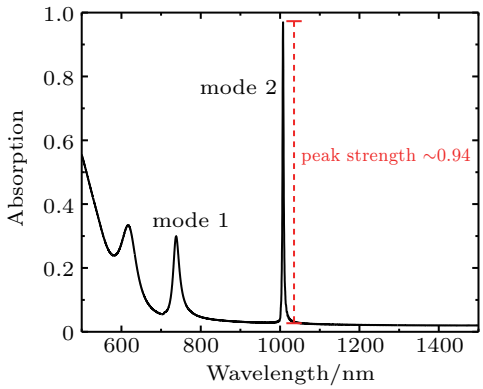


Fig. 2. The absorption spectrum of the structure in the near-infrared range, where $w = 380$ nm, $h_1 = 80$ nm, and the period is 1000 nm.

In order to better explain the two modes, we give the electric field distribution of the structure under the resonance wavelengths of modes 1 and 2 respectively. Figures 3(a) and 3(b) respectively show the electric field distributions of modes 1 and 2 in the X–Z plane along the center of the gold rhombus particles. It can be seen that the effective conversion of energy between the incident light and surface plasmons caused by grating coupling is the forming reason of the two modes. Simultaneously, the electric field enhancement of mode 2 is substantially stronger than that of mode 1, which explains the higher absorptivity of mode 2 in Fig. 2. In addition, it can also be seen from the electric field distribution

that the range of interaction between mode 2 and surrounding dielectric is wider than that of mode 1, which potentially indicates higher sensing sensitivity. Figures 3(c) and 3(d) respectively show the electric field distributions of the modes 1 and 2 on the upper surface of the gold film. It can be clearly observed that the energy of the incident light is transformed into the PSP propagating along the upper surface of the gold film. Different propagation patterns of PSP in the two modes correspond to two different diffraction orders of 2D grating. All the electric field distributions of the two modes show the characteristics of the PSP resonance, which fully confirms that the two modes are excited by 2D grating.

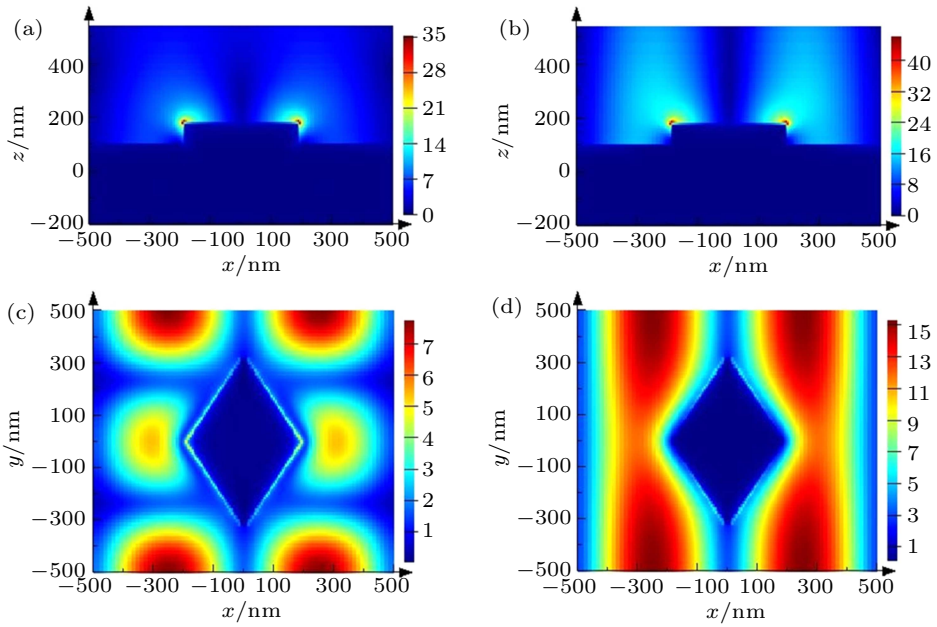


Fig. 3. Electric field distribution at the resonance wavelength of (a) mode 1 and (b) mode 2 in the X–Z plane along the center of the gold rhombus particles. Electric field distribution at the resonance wavelength of (c) mode 1 and (d) mode 2 on the upper surface of the gold film.

To further reveal the resonance mechanism caused by 2D grating coupling, we calculate the resonance wavelengths from the momentum matching equation at the interface between dielectric and metal. The momentum matching equation is given as

$$k_{x_\mathrm{light}} + k_{\mathrm{grating}} = k_{\mathrm{sp}}, \tag{1}$$

where k_{x_light} is the k-vector of the incident light in x-direction, k_{grating} is the additional momentum compensated by 2D grating, and k_{sp} is the k-vector of the surface plasmon. Specifically, we have

$$k_0 n \sin\varphi + \frac{2\pi}{P}\sqrt{p^2+q^2} = k_0\sqrt{\frac{\mathrm{Re}(\varepsilon_{\mathrm{m}})\cdot n_{\mathrm{a}}^2}{\mathrm{Re}(\varepsilon_{\mathrm{m}})+n_{\mathrm{a}}^2}}. \tag{2}$$

As shown in Eq. (2), $k_0 = 2\pi/\lambda$ is the propagation constant in free space, n_{a} is the RI of the analyte, ε_{m} is the complex dielectric constant of the gold, φ is the incident angle, P is the 2D grating period, p and q are the diffraction orders of 2D gratings and are integers. In the case of normal incidence, equation (2) can be reduced to

$$\lambda_{\mathrm{res}} = \frac{P}{\sqrt{p^2+q^2}}\sqrt{\frac{\mathrm{Re}(\varepsilon_{\mathrm{m}})\cdot n_{\mathrm{a}}^2}{\mathrm{Re}(\varepsilon_{\mathrm{m}})+n_{\mathrm{a}}^2}}, \tag{3}$$

where λ_{res} is the resonance wavelength. Two conclusions can be drawn from Eq. (3): (i) the resonance wavelength moves to the short wavelength with the increase of diffraction orders; (ii) the resonance wavelength red shifts linearly with the increase of the 2D grating period. Therefore, modes 1 and 2 correspond to diffraction orders (p, q) = (1, 1) and (1, 0), respectively.

Figure 4(a) shows the structure absorption spectra of different 2D grating periods with a step interval of 100 nm when w and h_1 are 380 nm and 80 nm, respectively. It can be observed that with the increase of the period of the 2D grating, the resonance wavelength of mode 2 shows a good linear shift to the long wavelength direction. This is consistent with the prediction of Eq. (3). Figure 4(b) shows a comparison of simulation results and theoretical analysis about the resonance wavelengths of mode 2 (first-order diffraction) for different 2D grating periods. The simulation results of resonance wavelengths are from Fig. 4(a). One can see that the simulation results are almost identical with the theoretical analysis. The differences of several wavelengths in simulation and analysis are caused by the n in Eq. (3). Due to the existence of 2D grating units, the n in Eq. (3) should actually be the effective refractive index of the arrays and analyte. Obviously, such an error can be seen as a perturbation in our structure. It is noteworthy that the discussion above of the plasmonic responses is based on the polarization direction of the incident light along the short diagonal direction of the rhombus. However, the ex-

citation along the long diagonal direction has little effect on the position of the resonance wavelengths since the periods of the 2D grating are equal in the X and Y directions.

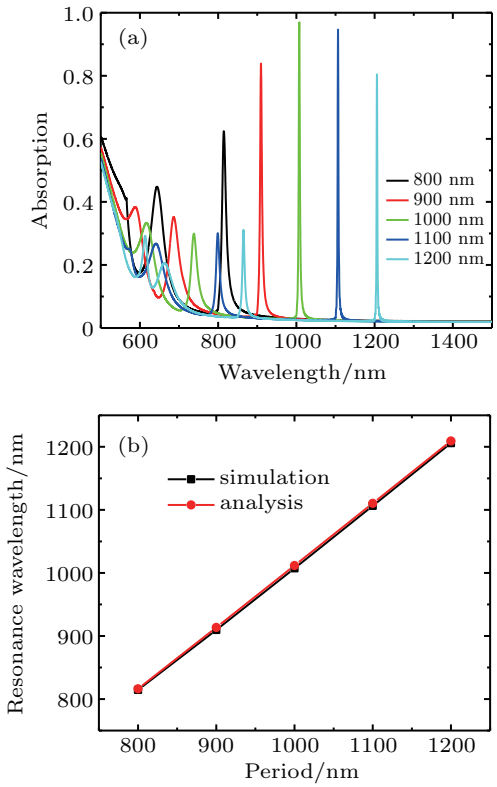


Fig. 4. (a) Absorption spectra of the structure with different 2D grating periods when w and h_1 are 380 nm and 80 nm, respectively. (b) Comparison between simulation results and theoretical analysis about the resonance wavelengths of mode 2 for different 2D grating periods.

4. Sensing performance of the structure

For the purpose of using this structure for RI sensing, mode 2 with perfect absorption and narrow FWHM is mainly discussed below. We firstly optimize the geometric parameters of the structure, the tolerance for geometric parameters suitable for RI sensing can be understood. Figure 5 illustrates the influence of the geometric parameters of the rhombus particles on mode 2 when the 2D grating period is 1000 nm. It can be clearly observed that the resonance wavelengths remain unchanged with the increase of the height of 2D grating units, while FWHM becomes wider. It is also observed that the absorptivity increases first and then decreases with the increase of h_1. Similar phenomena can also be seen from the change of the side length of the rhombus particles, where w changes from 200 nm to 500 nm with a step interval of 60 nm as shown in Fig. 5(b). The above phenomena are apparent, since too small 2D grating particles will lose the function of composing 2D grating, and too large particles will affect the propagation of PSP on the upper surface of the gold film. Therefore, when the period of 2D grating is 1000 nm, the most suitable geometric parameters for RI sensing are $h_1 = 80$ nm and $w = 380$ nm. It should be pointed out that the size of 2D grating units needs to be optimized under different period conditions. For example, figure 4(a) shows the absorption spectra of the structure when h_1 and w are 80 nm and 380 nm, respectively. Obviously, with the increasing 2D grating period, the absorptivity increases to the maximum value and then decreases, which can not be stabilized at a higher value in a wide period range.

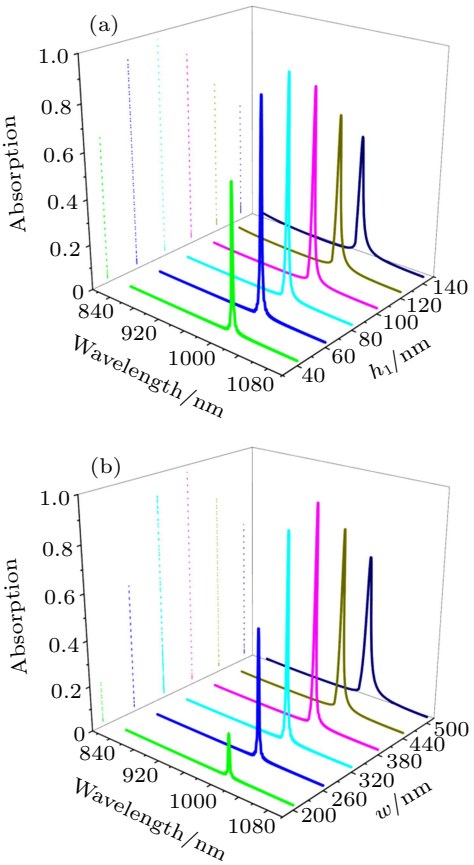


Fig. 5. (a) The absorption spectra of the structure when the period and w are 1000 nm and 380 nm, respectively, where h_1 varies from 80 nm to 140 nm in step of 20 nm. (b) The absorption spectra of the structure when the period and h_1 are 1000 nm and 80 nm, respectively, where w varies from 200 nm to 500 nm in step of 60 nm.

The RI sensing based on SPR is realized by establishing the corresponding relationship between the resonance peak position and the analyte RI. Therefore, the sensitivity (S) can be defined as the change of the resonance peak position under the change of unit RI of analyte, i.e., $S = \Delta\lambda/\Delta n$. The narrower the FWHM of the resonance peak used for sensing, the higher the spectral resolution can be obtained, and then the figure of merit, FOM $= S/\text{FWHM}$, can be derived. The S and FOM are two important physical parameters to describe the SPR-based RI sensing performance. The higher the values of S and FOM, the better the sensing performance of the RI sensor.

The changes in resonance wavelength corresponding to the analyte RI from 1.33 to 1.40 with a step interval of 0.01 are shown in Fig. 6(a), with the optimized geometrical parameters as already discussed above. It can be clearly observed that there is a good linear relationship between the resonance

peak position and the analyte RI. Meanwhile, the absorptivity at resonance wavelength remains at a high value (~ 0.98) and the FWHM is almost unchanged. Figure 6(b) is a good description of the above characteristics, which shows the resonance wavelength and peak strength versus the analyte RI. The corresponding slope of the curve (shown in Fig. 6(b) by the black line) represents the S of 1006 nm/RIU, and the FOM of 212.6 RIU^{-1} can be achieved considering its FWHM ~ 4.73 nm. Compared with the plasmonic RI sensors in recent reports, the FOM of this plasmonic sensor is quite high in the sensing range of near liquid RI.[39–42]

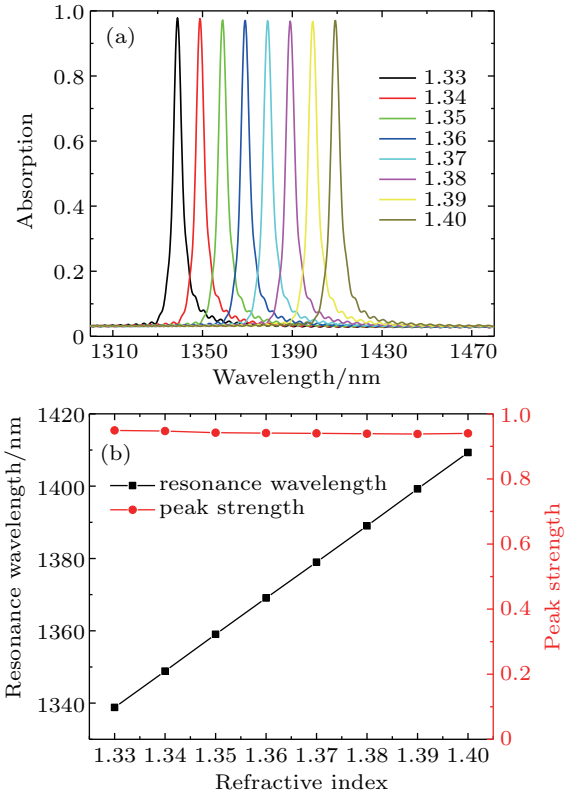


Fig. 6. (a) The absorption spectra of the structure with optimized geometrical parameters for different analyte RI. (b) Resonance wavelength and peak strength versus the RI of analyte.

The advantages of this plasmonic RI sensor are not only reflected in the high S and FOM, but also in the ultra wide RI sensing range. Figure 7(a) shows the absorption spectra of the structure when the analyte RI varies from 1.0 to 2.4 in step interval of 0.2 under the optimized geometric parameters. It can be observed that even in such a wide range of analyte RI changes, mode 2 does not lose its ability for RI sensing (still maintaining a narrow FWHM and a high peak strength). Although the peak strength of mode 2 decreases when the analyte RI exceeds 1.8, mode 2 is still capable of sensing when the analyte RI exceeds 2.4. A good linear relationship between resonance wavelength and analyte RI in an ultra wide sensing range keeps the sensitivity at a high value of 1006 nm/RIU. In addition, it can also be observed from Fig. 7(a) that mode 1 also has certain sensing capability, but obviously mode 1 shows lower S and FOM than mode 2. The RI sensing of mode 1 can be combined with mode 2 to improve the sensing accuracy. Figure 7(b) shows the FOM and FWHM of mode 2 corresponding to Fig. 7(a) as a function of the analyte RI. It can be seen that with the increase of the analyte RI, FOM gradually decreases due to the increase of FWHM. Here, the maximum FOM that mode 2 can achieve is 305.7 RIU^{-1}, which is nearly within the RI sensing range of the analyte being gas.

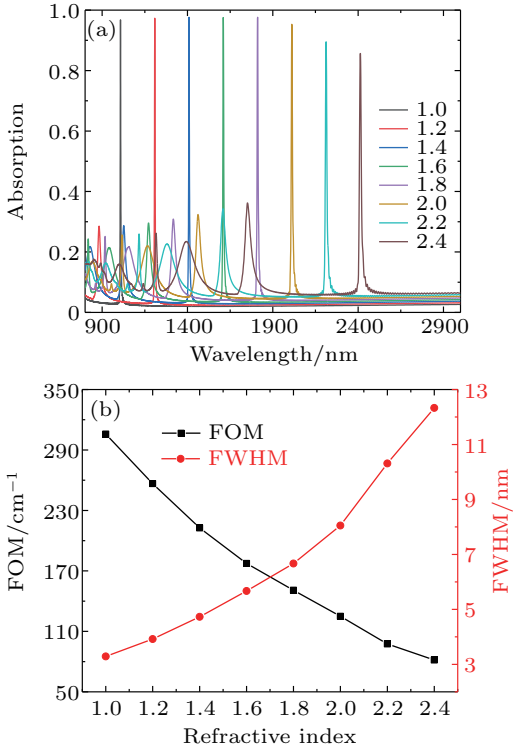


Fig. 7. (a) The absorption spectra of the structure when the analyte RI varies from 1.0 to 2.4 in step interval of 0.2. (b) The FOM and FWHM of mode 2 in the ultra wide analyte RI range.

5. Conclusion

In summary, a plasmonic RI sensor based on 2D metal grating composed of rhombus particles on a gold film is presented. The detailed discussion of structure plasmonic response, including simulation and theoretical analysis, fully demonstrates the effective energy coupling between the surface plasmons and incident light. A perfect absorption occurs via the first-order diffraction of the 2D mental grating, and the extremely narrow FWHM and high peak strength make it very suitable for RI sensing. After optimizing the geometrical parameters of the absorption spectra, the S and the highest FOM of the structure are 1006 nm/RIU and 305.7 RIU^{-1}, respectively. Moreover, a 1.0 to 2.4 ultra wide RI sensing range is one of the promising advantages of this plasmonic sensor, which fully covers the analyte of gas and liquid. This plasmonic RI sensor can be widely used in biological and chemical fields due to its stable sensing performance in an ultra wide RI sensing range.

References

[1] Liu G, Liu X, Chen J, Li Y, Shi L, Fu G and Liu Z 2019 *Sol. Energy Mater. Sol. Cells* **190** 20
[2] Li J, Chen X, Yi Z, Yang H, Tang Y, Yi Y, Yao W, Wang J and Yi Y 2020 *Mater. Today Energy* **16** 100390
[3] Liu Z, Liu G, Huang Z, Liu X and Fu G 2018 *Sol. Energy Mater. Sol. Cells* **179** 346
[4] Li J, Chen Z, Yang H, Yi Z, Chen X, Yao W, Duan T, Wu P, Li G and Yi Y 2020 *Nanomaterials* **10** 257
[5] Ge R, Yan B, Xie J, Liu E, Tan W and Liu J 2020 *J. Magn. Magn. Mater.* **500** 166367
[6] Huo Z, Liu E and Liu J 2020 *Chin. Opt. Lett.* **18** 030603
[7] Zhao H, Xie J and Liu J 2020 *Appl. Phys. Express* **13** 022007
[8] Hou T, Ge R, Tan W and Liu J 2020 *J. Phys. D: Appl. Phys.* **53** 075104
[9] Guo Z, Yan B and Liu J 2020 *J. Opt.* **22** 035002
[10] Li M, Feng W, Su W and Wang X 2020 *Int. J. Electrochem. Sci.* **15** 526
[11] Su W, Feng W, Cao Y, Chen L, Li M and Song C 2018 *Int. J. Electrochem. Sci.* **13** 6005
[12] Yan Y, Yang H, Yi Z, Xian T, Li R and Wang X 2019 *Desalin. Water Treat.* **170** 349
[13] Yan Y, Yang H, Yi Z, Wang X, Li R and Xian T 2020 *Environ. Eng. Sci.* **37** 64
[14] Wang Y, Jiang F, Chen J, Sun X, Xian T and Yang H 2020 *Nanomaterials* **10** 178
[15] Gao H, Zhao X, Zhang H, Chen J, Wang S and Yang H 2020 *J. Electron. Mater.* **49** 5248
[16] Zheng C, Yang H, Cui Z, Zhang H and Wang X 2017 *Nanoscale Res. Lett.* **12** 608
[17] Huan H, Jile H, Tang Y, Li X, Yi Z, Gao X, Chen X, Chen J and Wu P 2020 *Micromachines* **11** 309
[18] He W, Feng Y, Da Z, Balmakou A, Khakhomov S, Deng Q and Wang J 2020 *IEEE Sens. J.* **20** 1801
[19] Wang J, Yang L, Da Z, He W and Zheng G 2019 *IEEE Photon. Technol. Lett.* **31** 561
[20] Ma J, Liu D, Wang J and Feng Y 2018 *Acta Phys. Sin.* **67** 094102 (in Chinese)
[21] Shao H, Chen C, Wang J, Pan L and Sang T 2017 *J. Phys. D: Appl. Phys.* **50** 384001
[22] Wu H, Jile H, Chen Z, Xu D, Yi Z, Chen X, Chen J, Yao W, Wu P and Yi Y 2020 *Micromachines* **11** 189
[23] Tong H, Xu Y, Su Y and Wang X 2019 *Results Phys.* **14** 102460
[24] Wang X, Pang Z, Yang H and Qi Y 2019 *Results Phys.* **14** 102446
[25] Liu X, Liu G, Tang P, Fu G, Du G, Chen Q and Liu Z 2018 *Carbon* **140** 362
[26] Liu G, Chen J, Pan P and Liu Z 2019 *IEEE J. Sel. Top. Quantum Electron.* **25** 4600507
[27] Wang Y, Chen Z, Xu D, Yi Z, Chen X, Chen J, Tang Y, Wu P, Li G and Yi Y 2020 *Results Phys.* **16** 102951
[28] Qi Y, Zhou P, Zhang T, Zhang X, Wang Y, Liu C, Bai Y and Wang X 2019 *Results Phys.* **14** 102506
[29] Qi Y, Zhang X, Zhou P, Hu B and Wang X 2018 *Acta Phys. Sin.* **67** 197301 (in Chinese)
[30] Zhang X, Qi Y, Zhou P, Gong H, Hu B and Yan C 2018 *Photonic Sens.* **8** 367
[31] Wang X, Wu Y, Wen X, Zhu J, Bai X, Qi Y and Yang H 2020 *Opt. Quantum Electron.* **52** 238
[32] Wu Y, Wang X, Wen X, Zhu J, Bai X, Jia T, Yang H, Zhang L and Qi Y 2020 *Phys. Lett. A* **384** 126544
[33] Wang X, Zhu J, Wu Y, Xu Y, Su Y, Zhang L, Qi Y, Wen X and Yang H 2020 *Results Phys.* **17** 103175
[34] Chen J, Wang X, Tang F, Ye X, Yang L and Zhang Y 2020 *Results Phys.* **16** 102867
[35] Liu C, Yang L, Liu Q, Wang F, Sun Z, Sun T, Mu H and Chu P K 2018 *Plasmonics* **13** 779
[36] Liu C, Wang J, Wang F, Su W, Yang L, Lv J, Fu G, Li X, Liu Q, Sun T and Chu P K 2020 *Opt. Commun.* **464** 125496
[37] Liu C, Wang J, Jin X, Wang F, Yang L, Lv J, Fu G, Li X, Liu Q, Sun T and Chu P K 2020 *Optik (Stuttg).* **207** 164466
[38] Chen J, Yuan J, Zhang Q, Ge H, Tang C, Liu Y and Guo B 2018 *Opt. Mater. Express* **8** 342
[39] Chen J, Zhang Q, Peng C, Tang C, Shen X, Deng L and Park G 2018 *IEEE Photon. Technol. Lett.* **30** 728
[40] Chen J, Fan W, Mao P, Tang C, Liu Y, Yu Y and Zhang L 2017 *Plasmonics* **12** 529
[41] Chen J, Nie H, Peng C, Qi S, Tang C, Zhang Y, Wang L and Park G S 2018 *J. Light. Technol.* **36** 3481
[42] Wang X, Zhu J, Tong H, Yang X, Wu X, Pang Z, Yang H and Qi Y 2019 *Chin. Phys. B* **28** 044201
[43] Guner H, Ozgur E, Kokturk G, Celik M, Esen E, Topal A E, Ayas S, Uludag Y, Elbuken C and Dana A 2017 *Sens. Actuators B Chem.* **239** 571
[44] Sun P, Zhou C, Jia W, Wang J, Xiang C, Xie Y and Zhao D 2020 *Opt. Commun.* **459** 124946
[45] Sui B, Xu Y, Wang Z, Zhang C, Qin L, Li X and Wu S 2019 *Opt. Express* **27** 38382
[46] Wang X, Zhu J, Wen X, Wu X, Wu Y, Su Y, Tong H, Qi Y and Yang H 2019 *Opt. Mater. Express* **9** 3079
[47] Johnson P B and Christy R W 1972 *Phys. Rev. B* **6** 4370